Resonance parameters of the rho-meson from asymmetrical lattices

C. Pelissier and A. Alexandru

Resonance parameters of the rho-meson from asymmetrical lattices

C. Pelissier, A. Alexandru

Physics Department, The George Washington University, Washington, DC 20052, USA

We present a lattice QCD calculation of the parameters of the ρ meson decay. The study is carried out on spatially asymmetric boxes using nHYP-smeared clover fermions with two mass-degenerate quark flavors. Our calculations are carried out at a pion mass $m_\pi = 304(2)$ MeV on the set of lattices $V = 24^2 \times \eta 24 \times 48$ with $\eta = 1.0, 1.25$, and 2.0 with lattice spacing $a = 0.1255(7)$ fm. The resonance mass $m_\rho = 827(3)(5)$ MeV and coupling constant $g_{\rho\pi\pi} = 6.67(42)$ are calculated using the P-wave scattering phase shifts. We construct a 2×2 correlation matrix to extract the energy of the scattering states and compute the phase shifts using the finite volume formula. By varying the degree of asymmetry, we are able to compute a set of phase shifts that are evenly distributed throughout the spectral region where the ρ decays.

I. INTRODUCTION

The study of multi-particle systems is an important step for lattice QCD and our understanding of the strong force. Experimentally, the interaction of elementary particles is studied using scattering methods. Due to better algorithms, more efficient codes, and an increase in computational resources, it is finally possible to use lattice QCD to compute scattering observables. Of particular interest are the scattering channels that exhibit resonances. In this work, we focus on the light vector meson $\rho(770)$ seen as a resonance in the elastic scattering of two-pions in the $I^G(J^{PC}) = 1^+(1^{--})$ channel.

Currently, the method of choice to carry out lattice studies of scattering phase shifts is the Lüsher method [1–4]. Lüsher showed that scattering phase shifts can be computed from the spectrum of two-particle states on a torus. This method circumvents the "Maiani-Testa no-go theorem" for Euclidean field theories [5]. To measure scattering phase shifts then requires the computation of the energies of the two-particle states. While it is known how to compute the energies of the scattering states, the task can be quite challenging and is computationally costly. In the case of the ρ decay, as the physical pion mass is approached, the scattering states get closer together, and we have to carefully disentangle the relevant two-pion states. Additionally, when the four-pion states become dynamically relevant, the formula is no longer valid.

Lüsher's formula was developed for lattices with cubic symmetry. Two notable extensions were worked out: (1) systems with non-zero total momentum where the cubic symmetry is lost due to the relativistic boost to the center-of-mass frame [6] and (2) systems with zero total momentum on asymmetrical lattices [7, 8]. The first method can be used to investigate the ρ decay on lattices where the zero-momentum ρ cannot decay due to kinematical constraints. This was used recently to study the ρ resonance [9–11]. Using this method, different phase shifts can be extracted by varying the total momentum of the system. While it has been successful for studying the ρ resonance, the ability to tune the momentum of the two-pion system is limited by the finite step size of the momenta.

In this work we chose to use the second extension. This method offers a finer control over the two-pion momentum. With a finer control over the momentum, it is possible to map out narrower resonances, and as will be discussed later, the overall increase in computational cost is not that significant. Another reason for using asymmetrical lattices is that the projection onto the relevant irreducible representation can be performed cleanly. This projection is always performed in the center-of-mass, which coincides with the lattice frame when the interpolators have zero momentum. For systems with non-zero momentum, the boost mixes representations, and we have to rely on dynamics to disentangle the states of interest.

In this work we employ nHYP-smeared clover fermions with two mass-degenerate quarks. The simulation is carried out with a pion mass $m_\pi = 304(2)$ MeV at a lattice spacing $a = 0.1255(7)$ fm. We construct a 2×2 correlation matrix and extract the ground and first excited state energies on dynamically generated ensembles of 300 gauge configurations for the three lattice volumes

$$V = 24^2 \times \eta 24 \times 48 , \quad \eta = 1.0, 1.25, 2.0 . \tag{1}$$

We extract six scattering phase shifts well distributed throughout the resonance region and compute the resonance mass and coupling constant. The methods used here were first tested on a set of quenched configurations for similar quark masses and lattice sizes [12].

The paper is organized as follows: In Section II we describe the methods used and collect the relevant formulas. In Section III we present our results for the two-pion spectrum, compute the phase shifts, extract the resonance parameters, and compare our results with other studies. In Section IV we present our conclusions and discuss future plans.

II. METHODS

A. Phase shift formulas

To compute the elastic scattering phase shifts, we use the well-known Lüsher's formula [1–4]. In particular, we make use of its extension to asymmetrical lattices [7, 8]. In the following we list the relevant formula needed to determine the scattering phase shifts $\delta_l(k)$ for two pions with back-to-back momentum in the angular momentum $l = 1$ channel.

In this work we consider lattices with one spatial direction elongated. Since we work on a spatial torus, the symmetry group for zero-momentum states is reduced from $SO(3)$ to a discrete subgroup. In this case the relevant symmetry group is D_{4h}. For concreteness we take the z-direction to be elongated. The decomposition of the irreducible representations of $SO(3)$ into D_{4h} are listed in Table I. From the table we see that $l = 1$ is the lowest angular momentum mode which couples to the A_2^- and E^- representations; therefore, either representation is suitable. In the following we present the formula for these two channels.

Following [8], we introduce the generalized zeta functions

$$\mathcal{Z}_{lm}(s, q^2; \eta_2, \eta_3) = \sum_{\mathbf{n} \in \mathbb{Z}^3} \frac{\mathcal{Y}_{lm}(\tilde{\mathbf{n}})}{(\tilde{\mathbf{n}}^2 - q^2)^s} \qquad (2)$$

where $\mathcal{Y}_{lm}(\tilde{\mathbf{n}})$ are the harmonic polynomials

$$\mathcal{Y}_{lm}(\tilde{\mathbf{n}}) = \tilde{n}^l Y_{lm}(\Omega_{\tilde{\mathbf{n}}}) \qquad (3)$$

and

$$\tilde{\mathbf{n}} = (n_1, n_2/\eta_2, n_3/\eta_3), \quad \mathbf{n} \in \mathbb{Z} . \qquad (4)$$

The series in Eq. (2) is convergent for $\mathrm{Re}\, 2s > l + 3$ and can be analytically continued to the half plane $\mathrm{Re}\, 2s > 1/2$. To compute the scattering phase shifts, we need to evaluate $\mathcal{Z}_{lm}(s = 1, q^2; \eta_2, \eta_3)$. The details are given in Appendix A. The parameter q is related to the invariant energy W of the two-pion system through the relation

$$q = \frac{kL}{2\pi} \qquad (5)$$

where k, the pion "momentum", is determined by

$$W = 2\sqrt{m_\pi^2 + k^2} . \qquad (6)$$

The 3D torus geometry and spatial volume is $V = L \times \eta_2 L \times \eta_3 L$. For notational simplicity, we also introduce the quantity

$$\mathcal{W}_{lm}(1, q^2; \eta_2, \eta_3) = \frac{\mathcal{Z}_{lm}(1, q^2; \eta_2, \eta_3)}{\pi^{3/2} \eta_2 \eta_3 q^{l+1}} . \qquad (7)$$

Since our lattices are elongated only in one direction, we set $\eta_2 = 1$ and $\eta_3 \equiv \eta \geq 1$. The phase shift formula for

TABLE I: Resolution of the $2J + 1$ spherical harmonics into the irreducible representations of O_h and D_{4h}.

J	O_h	D_{4h}
0	A_1^+	A_1^+
1	F_1^-	$A_2^- \oplus E^-$
2	$E^+ \oplus F_2^+$	$A_1^+ \oplus B_1^+ \oplus B_2^+ \oplus E^+$
3	$A_2^- \oplus F_1^- \oplus F_2^-$	$A_2^- \oplus B_1^- \oplus B_2^- \oplus 2E^-$
4	$A_1^+ \oplus E^+ \oplus F_1^+ \oplus F_2^+$	$2A_1^+ \oplus A_2^+ \oplus B_1^+ \oplus B_2^+ \oplus 2E^+$

the two representations are then given by

$$\mathbf{A_2^-} : \quad \cot \delta_1(k) = \mathcal{W}_{00} + \frac{2}{\sqrt{5}} \mathcal{W}_{20} , \qquad (8)$$

$$\mathbf{E^-} : \quad \cot \delta_1(k) = \mathcal{W}_{00} - \frac{1}{\sqrt{5}} \mathcal{W}_{20} , \qquad (9)$$

where contributions from angular momenta $l \geq 3$ are assumed to be negligible.

We note that our formulation is slightly different than [8], which defines the lattice volume as $V = \eta_1 L \times \eta_2 L \times L$. The phase shift formulas in either case are equivalent. Additionally, our formula for the E^- channel differs by the exclusion of the term $\pm \sqrt{3/10}(\mathcal{W}_{22} + \mathcal{W}_{2-2})$, which vanishes due to symmetry under rotations around the elongated direction.

Lastly, we consider the case of a cubic lattice. The symmetry group is O_h, and the relevant representation is F_1^- (see Table I). In this case $\mathcal{W}_{20}$ vanishes, Eq. (8) and Eq. (9) become equivalent, and the phase shift formula is given by setting the right hand side equal to $\mathcal{W}_{00}$.

B. Selecting lattices

In order to extract the resonance parameters for ρ, we need to compute the scattering phase shifts in the spectral region where the resonance appears. To minimize statistical errors, it is preferable to compute the phase shifts using the lowest lying states in the channel. To achieve this, we have to select appropriate lattice volumes and, for practical purposes, make a selection which is computationally economic. This choice is difficult since the resonance mass and coupling constant are generally not known a priori for unphysical pion masses. However, using recent lattice results [9, 11, 13] and predictions from unitarized chiral perturbation theory [14], a reasonably good guess can be made. In the following we describe the method we used to select lattices.

To estimate the two-pion energies, we use the effective range formula [15]

$$\cot \delta_1(W) = \frac{6\pi}{g_{\rho\pi\pi}^2} \frac{W(m_\rho^2 - W^2)}{\left(\frac{W^2}{4} - m_\pi^2\right)^{3/2}} , \qquad (10)$$

which is known to parameterized the ρ resonance well at the physical pion mass. Using the equation above together with Eqs. (8) and (9), we can compute the expected spectrum as a function of η provided we can estimate the values of m_ρ and $g_{\rho\pi\pi}$. From recent lattice studies we know that the coupling constant has little pion mass dependence and is close to the physical value $g_{\rho\pi\pi} \approx 6$ for pion masses $m_\pi < 350$ MeV [9, 11, 13]. As a result, we start with the assumption that $g_{\rho\pi\pi} = 6$. To estimate the value of m_ρ, we use the result from unitarized chiral perturbation theory which shows reasonable agreement with the lattice results [14]. Note that this picture can be refined as we collect data from lattice simulations. When choosing subsequent lattices, we use estimates for m_ρ and $g_{\rho\pi\pi}$ based on the available lattice data.

In Fig. 1 we plot the expected spectrum for a pion mass of 300 MeV. Note that the two-dimensional E^- representation corresponds to the two states with non-zero back-to-back momentum in the transversal directions, and the A_2^- representation is the one-dimensional representation corresponding to the state with the momentum along the longitudinal/elongated direction. For the E^- representation the spectrum depends very little on η. The reason is that the relative momentum of the two-pion state depends on the size of the transversal direction, which does not change. Thus, computing the energy of the states in the E^- representation will produce phase shifts very similar to the ones on a cubic lattice. The A_2^- representation shows a strong dependence on the value of η and offers good control over the value of the ground and first excited state energies. To generate additional phase shifts, one then needs to work in the A_2^- channel and select appropriate values of η. We see that by choosing $\eta = 1$, 1.25, and 2.0, we should get a good scan of the resonance region.

Lastly, we make a few remarks about our choice to use lattices with a single direction elongated. It may seem
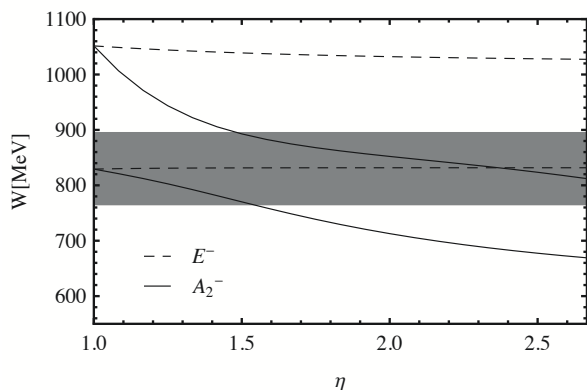

FIG. 1: Estimated spectrum for $m_\pi = 300$ MeV, $g_{\rho\pi\pi} = 6$, and $m_\rho = 830$ MeV. The lattice size is set to $L = 3$ fm. The two curves indicate the ground and first excited states. The shaded region is the resonance region, i.e., $m_\rho \pm \Gamma_\rho$.

that a better choice for these types of studies are orthorhombic lattices, i.e., lattices in which all three sides have different lengths. In this case six different phase shifts can be computed from one ensemble using only the ground and first excited state energies. Choosing appropriate values for L, η_2, and η_3, we could get all of these phase shifts in the resonance region. Since the computational effort scales with $V^{5/4}$ [16], the computational cost is $(\eta_2\eta_3)^{5/4} \times \tau$ where τ denotes the cost for the cubic lattice. If instead we choose a lattice with only one direction elongated and generate the two ensembles with $\eta = \eta_2$ and $\eta = \eta_3$, the cost is $(\eta_2^{5/4} + \eta_3^{5/4}) \times \tau$. The overall computational cost of the two choices is similar when the elongation parameters $\eta_{2,3}$ are small. Additionally, using two different ensembles reduces the correlation between phase shifts and allows for studies of finite volume effects of other observables. In light of these considerations, we choose to generate lattices with only a single direction elongated.

C. Variational analysis

To compute the low-lying two-pion energies with the quantum numbers $I^G(J^{PC}) = 1^+(1^{--})$ of the ρ, we employ the variational method proposed by Lüscher and Wolff [17]. We use a two-dimensional variational basis and construct the correlation matrix

$$C(t)_{ij} = \langle \mathcal{O}_i(t)\mathcal{O}_j^\dagger(0)\rangle \tag{11}$$

to extract the ground and first excited states. We compute the eigenvalues of

$$C(t_0)^{-1/2}C(t)C(t_0)^{-1/2}\psi^{(n)}(t,t_0) = \lambda^{(n)}(t,t_0)\psi^{(n)}(t,t_0) \tag{12}$$

for each time slice t. The two-pion energies are then determined from the long-time behavior of the eigenvalues [18]

$$\lambda^{(n)}(t,t_0) \propto e^{-E_n t}(1 + \mathcal{O}(e^{-\Delta E_n t})), \quad n = 1, 2 \tag{13}$$

where $\Delta E_n = E_3 - E_n$. For the variational basis we use the interpolators

$$\mathcal{O}_1 = \frac{1}{\sqrt{2}}\left\{\pi^+(\mathbf{p}_z)\pi^-(-\mathbf{p}_z) - \pi^-(\mathbf{p}_z)\pi^+(-\mathbf{p}_z)\right\} \tag{14}$$

$$\mathcal{O}_2 = \sum_{\mathbf{x}}\frac{1}{\sqrt{2}}\left\{\bar{u}(x)\gamma_3 u(x) - \bar{d}(x)\gamma_3 d(x)\right\} \tag{15}$$

where $\mathbf{p}_z = \frac{2\pi}{\eta L}\hat{z}$ is the lowest lattice momentum in the elongated direction and

$$\pi^-(\mathbf{p}) = \sum_{\mathbf{x}}\bar{u}(\mathbf{x})\gamma_5 d(\mathbf{x})e^{i\mathbf{p}\mathbf{x}}, \tag{16}$$

$$\pi^+(\mathbf{p}) = \sum_{\mathbf{x}}\bar{d}(\mathbf{x})\gamma_5 u(\mathbf{x})e^{i\mathbf{p}\mathbf{x}}. \tag{17}$$

Lastly, we note that as defined above $\mathcal{O}_1$ and $\mathcal{O}_2$ are hermitian and anti-hermitian, respectively.

D. Evaluation of the correlation matrix

To evaluate the correlation matrix, one needs to compute the following diagrams:

$$C_{11}(t)$$

$$\square \quad \square \quad \boxtimes \quad \boxtimes \quad \boxtimes\!\!\!\boxtimes \quad \backslash\!\backslash$$

$$C_{12}(t) \qquad C_{21}(t) \qquad C_{22}(t)$$

$$\triangledown \quad \triangledown \quad \triangle \quad \triangle \quad \lozenge$$

Above, we used a compressed notation; more explicitly, we have

$$
\begin{aligned}
&\overset{(-\boldsymbol{p},t_f)\ \ (\boldsymbol{p},t_f)}{\underset{(-\boldsymbol{p},t_i)\ \ (\boldsymbol{p},t_i)}{\overset{\gamma_5\ \ \ \ \gamma_5}{\underset{\gamma_5\ \ \ \ \gamma_5}{\square}}}} = \ \mathrm{Tr}\,[e^{-i\boldsymbol{p}}\gamma_5 M^{-1}(t_i,t_i)e^{i\boldsymbol{p}}\gamma_5 M^{-1}(t_i,t_f)\times \\
&\qquad\qquad e^{i\boldsymbol{p}}\gamma_5 M^{-1}(t_f,t_f)e^{-i\boldsymbol{p}}\gamma_5 M^{-1}(t_f,t_i)]\,,\quad (18)
\end{aligned}
$$

where the square matrices

$$
\begin{aligned}
(\gamma_5)_{\boldsymbol{x},a,\alpha;\boldsymbol{y},b,\beta} &\equiv\ \delta(\boldsymbol{x}-\boldsymbol{y})(\gamma_5)_{ab}\delta_{\alpha\beta}\,, \\
(e^{i\boldsymbol{p}})_{\boldsymbol{x},a,\alpha;\boldsymbol{y},b,\beta} &\equiv\ e^{i\boldsymbol{p}\boldsymbol{x}}\delta(\boldsymbol{x}-\boldsymbol{y})\delta_{ab}\delta_{\alpha\beta}\,, \qquad (19) \\
M^{-1}(t_f,t_i)_{\boldsymbol{x},a,\alpha;\boldsymbol{y},b,\beta} &\equiv\ M^{-1}(\boldsymbol{x},t_f,a,\alpha;\boldsymbol{y},t_i,b,\beta)\,,
\end{aligned}
$$

have $12 \times N_s$ rows with N_s the number of points in a time slice. Above, M is the quark matrix and thus M^{-1} is the regular quark propagator. All four-point diagrams are defined in a similar manner. The diagrams with three points can be written using the following template:

$$
\begin{aligned}
&\overset{(\boldsymbol{0},t_f)}{\underset{\underset{(-\boldsymbol{p},t_i)\ \ (\boldsymbol{p},t_i)}{\gamma_5\ \ \ \ \ \gamma_5}}{\overset{\gamma_3}{\triangle}}} = \ \mathrm{Tr}\,[e^{-i\boldsymbol{p}}\gamma_5 M^{-1}(t_i,t_i)\times \\
&\qquad\qquad e^{i\boldsymbol{p}}\gamma_5 M^{-1}(t_i,t_f)\gamma_3 M^{-1}(t_f,t_i)]\,. \quad (20)
\end{aligned}
$$

For a given configuration, using the γ_5-hermiticity of the quark propagator, i.e., $M^{-1}(t,t')^\dagger = \gamma_5 M^{-1}(t',t)\gamma_5$, we can show that the four-point diagrams are purely real, and the three-point diagrams are purely imaginary. Moreover, using parity we can show that

$$
\left\langle \triangle \right\rangle_U = -\left\langle \triangle \right\rangle_U\,, \quad \left\langle \triangledown \right\rangle_U = -\left\langle \triangledown \right\rangle_U\,,
$$

$$
\left\langle \square \right\rangle_U = \left\langle \square \right\rangle_U\,, \quad \left\langle \boxtimes \right\rangle_U = \left\langle \boxtimes \right\rangle_U\,.
\quad (21)
$$

Time reversal symmetry allows us to connect the quark diagrams required for C_{12} with the ones for C_{21}. In particular, one can show that

$$
\left\langle \triangledown \right\rangle_U = \left\langle \triangle \right\rangle_U\,. \quad (22)
$$

Above we use $\langle\cdot\rangle_U$ to denote the average with respect to the gauge configurations. All together, the four components of the correlation matrix can be constructed from

$$
\begin{aligned}
C_{11}(t) &=\ \left\langle 2\,\square - 2\,\boxtimes + \boxtimes\!\!\!\boxtimes - \backslash\!\backslash \right\rangle_U\,, \\
C_{12}(t) &=\ -C_{21}(t) = \left\langle \triangledown \right\rangle_U\,, \qquad (23) \\
C_{22}(t) &=\ \left\langle \lozenge \right\rangle_U\,.
\end{aligned}
$$

Note that C_{12} and C_{21} are related. To save time, we compute only C_{21} and use it to determine C_{12}. C_{22} can be evaluated using standard methods, but the terms for C_{11} and C_{21} require the all-to-all propagator. As a result, they must be computed stochastically. Our calculation follows the steps described in a study by the CP-PACS collaboration [11]. We introduce a random $Z(4)$ noise time-slice vector ξ (with color and spinor components), satisfying the condition

$$
\left\langle \xi\xi^\dagger \right\rangle_\xi = \mathbb{1} \qquad (24)
$$

where $\mathbb{1}$ is the identity matrix in $12 \times N_s$ dimensions and $\langle\cdot\rangle_\xi$ denotes the average over the noise. Using these noise vectors, we define the time-slice vectors

$$
\begin{aligned}
u(t|\boldsymbol{p},t_2,\xi) &=\ M^{-1}(t,t_2)e^{i\boldsymbol{p}}\xi \qquad (25) \\
v(t|\boldsymbol{p}_1,t_1|\boldsymbol{p}_2,t_2,\xi) &=\ M^{-1}(t,t_1)e^{i\boldsymbol{p}_1}\gamma_5 u(t_1|\boldsymbol{p},t_2,\xi)\,.
\end{aligned}
$$

With the above definitions unbiased estimators for the quark diagrams for $C_{11}(t)$ and $C_{21}(t)$ can be constructed as

$$
\begin{aligned}
\square &=\ \left\langle v(t_f|\boldsymbol{p},t_i|-\boldsymbol{p},t_i,\xi)^\dagger e^{-i\boldsymbol{p}} v(t_f|\boldsymbol{p},t_f|\boldsymbol{0},t_i,\xi) \right\rangle_{\xi,U}\,, \\
\boxtimes &=\ \left\langle v(t_f|-\boldsymbol{p},t_i|\boldsymbol{p},t_i,\xi)^\dagger e^{-i\boldsymbol{p}} v(t_f|\boldsymbol{p},t_i|\boldsymbol{0},t_i,\xi) \right\rangle_{\xi,U}\,, \\
\boxtimes\!\!\!\boxtimes &=\ \Big\langle \left\langle u(t_f|\boldsymbol{0},t_i,\xi)^\dagger e^{-i\boldsymbol{p}} u(t_f|\boldsymbol{p},t_i,\xi) \right\rangle_\xi \times \\
&\qquad \left\langle u(t_f|\boldsymbol{0},t_i,\eta)^\dagger e^{i\boldsymbol{p}} u(t_f|-\boldsymbol{p},t_i,\eta) \right\rangle_\eta \Big\rangle_U\,, \\
\backslash\!\backslash &=\ \Big\langle \left\langle u(t_f|\boldsymbol{0},t_i,\xi)^\dagger e^{-i\boldsymbol{p}} u(t_f|-\boldsymbol{p},t_i,\xi) \right\rangle_\xi \times \\
&\qquad \left\langle u(t_f|\boldsymbol{0},t_i,\eta)^\dagger e^{i\boldsymbol{p}} u(t_f|\boldsymbol{p},t_i,\eta) \right\rangle_\eta \Big\rangle_U\,, \qquad (26) \\
\triangle &=\ \left\langle u(t_f|\boldsymbol{0},t_i,\xi)^\dagger \gamma_5\gamma_3 v(t_f|-\boldsymbol{p},t_i|\boldsymbol{p},t_i,\xi) \right\rangle_{\xi,U}\,, \\
\triangle &=\ \left\langle u(t_f|\boldsymbol{0},t_i,\xi)^\dagger \gamma_5\gamma_3 v(t_f|\boldsymbol{p},t_i|-\boldsymbol{p},t_i,\xi) \right\rangle_{\xi,U}\,.
\end{aligned}
$$

Lastly, we make a few comments on the variance of the stochastic estimators. As is common practice, we chose to use spin-color dilution. To check its effectiveness, we compared the variance of $C_{11}(t)$ and $C_{21}(t)$ with and without dilution in the temporal range where the fitting is performed. Using spin-color dilution, we found an order of magnitude decrease in the variance for the same
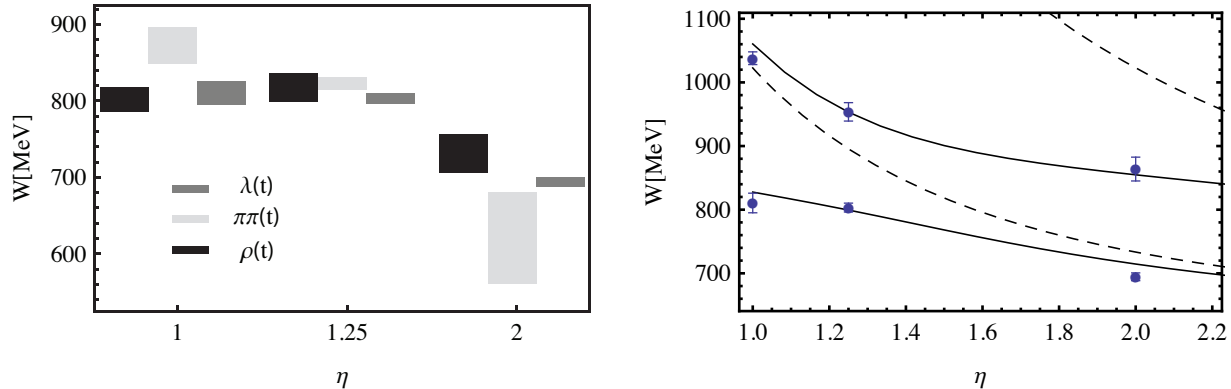
FIG. 2: Left panel: ground state energies for the three different elongations extracted using different methods. Right panel: ground and first excited state energies compared to the effective range formula using the parameters extracted from our fits. The dashed lines represent the expected two-pion energies in the absence of interaction, i.e., $W_n = 2\sqrt{m_\pi^2 + (2\pi n/\eta L)^2}$.

numerical effort. Another decision to make is the size of the noise ensembles. Using a simple model, we can show that the overall variance of the estimator is

$$\sigma^2 \approx \frac{\sigma_U^2}{N}\left(1 + \frac{\sigma_\xi^2/\sigma_U^2}{M}\right) \tag{27}$$

where σ_U^2 and σ_ξ^2 are the contributions to the overall variance from the gauge and noise fluctuations, N is the number of gauge configurations, and M the number of noises per configuration. In the temporal region where the fits were performed, we found that the ratio σ_ξ^2/σ_U^2 is small and that the variance is dominated by gauge fluctuations. As a result, the variance is not significantly decreased even after a single noise. This is similar to the results found by [11] where no substantial decrease in the variance was found after two noises. In this work, we also chose to use two noises.

The stochastic estimator requires thousands of inversions for each configuration making the numerical cost of the analysis comparable with the cost of generating the dynamical configurations. To carry out these calculations, we used our own GPU BiCGstab inverters [19].

III. RESULTS

A. Two-pion spectrum

To compute the two-pion spectrum, we generated three dynamical ensembles of 300 gauge configurations. We employed the Lüsher-Weiss action with $\beta = 7.1$, $\kappa = 0.1282$, and $u_0 = 0.868$. The simulation was carried out using nHYP-smeared clover fermions with two mass-degenerated quarks and the standard smearing parameters $\alpha_1 = 0.75$, $\alpha_2 = 0.6$, and $\alpha_3 = 0.3$ [20]. The spatial volume of the the three lattices was

$$24 \times 24 \times \eta 24\,, \quad \eta = 1.0\,, 1.25\,, 2.0\,, \tag{28}$$

with temporal extent $N_t = 48$. The lattice spacing for all three ensembles was determined to be $a = 0.1255(7)$ using the Sommer scale (see Appendix B), and the computed value for the pion mass was $m_\pi = 304(2)$ MeV.

We only computed the energies in the A_2^- channel since the energies in the E^- channel are not significantly different than those obtained in the F^- channel on the cubic lattice. The numerical values are listed in Table II. In the left panel of Fig. 2, we show the ground state energies obtained using solely the $\pi\pi$ and ρ interpolators, as well as the energy obtained using the variational method. The results show consistent behavior. As expected, the energy decreases as the lattice size is increased and the back-to-back momentum of the pions becomes smaller. Note that the individual correlators, extracted separately from $C_{11}(t)$ and $C_{22}(t)$, have larger error bars. For our fits we use the energies extracted using the variational method. This energy is expected to be lower than the one extracted using individual correlators; in our plot the central value for $\eta = 2$ seems to contradict this expectation, but the deviation is comparable with the error bar and most likely due to a statistical fluctuation.

In the right panel of Fig. 2, we show our results for the ground and first excited states, as well as the spectral behavior as predicted by the effective range formula Eq. (10) using our fit results. We see that the effective range formula describes the lattice data well and that the lattice data resolves clearly the effect of the pions' interaction.

B. Phase shifts and resonance parameters

To compute the resonance parameters, we evaluate the scattering formula Eq. (8) with the energies obtained for the ground and first excited states. The resonance mass and coupling constant are then computed by fitting the scattering phase shifts with the effective range formula
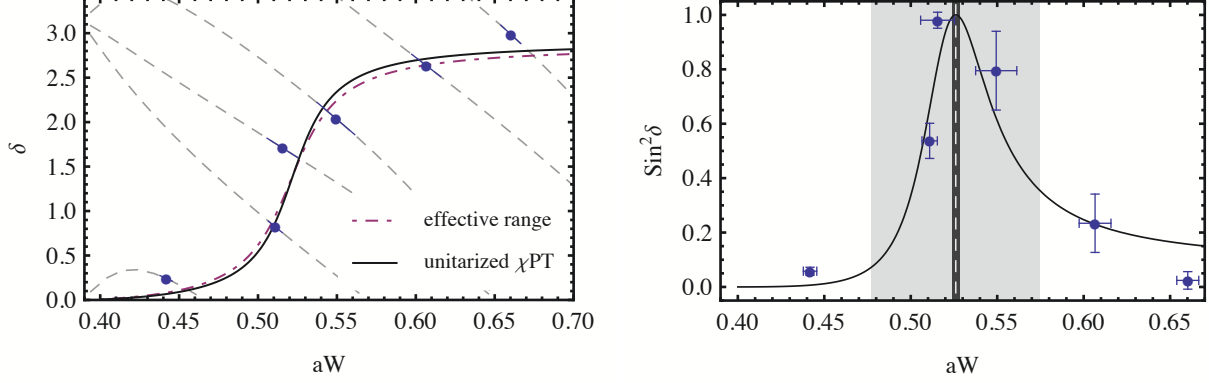
FIG. 3: Left panel: scattering phase shifts computed in this study, effective range formula fit, and the results from unitarized χPT [14]. The dashed lines describe the energy dependence of the phase shift according to Eq. (8). Right panel: cross section as a function of the center-of-mass energy. The dashed line indicates the ρ mass, the narrow dark band its error, and the shadowed box indicates the resonance region $m_\rho \pm \Gamma$.

given in Eq. (10). We use a correlated χ^2-fit since the energies for the ground and first excited states are extracted from the same ensemble and construct the covariance matrix with two-by-two blocks, one per ensemble.

Note that the standard χ^2 method needs to be modified for our fit: the statistical errors affect both x and y coordinates in our plot since the phase shifts are related to the energy. Referring to the left panel of Fig. 3, as the energy is varied the phase shifts move along the dashed lines indicated in the figure. The solid lines indicate the error bars obtained by varying the energy in the $W \pm \sigma_W$ interval. The χ^2 function is defined to be

$$\chi^2 = \frac{1}{2}\Delta^T C^{-1}\Delta \qquad (29)$$

where Δ is the difference vector

$$\Delta_i = W_i - W_i^0 , \qquad (30)$$

W_i indicates the computed value, and W_i^0 the value at the intersection of the dashed line and the fit curve.

The decay width is determined using the fit results and the relation

$$\Gamma = \frac{g_{\rho\pi\pi}^2}{6\pi} \frac{\left(m_\rho^2/4 - m_\pi^2\right)^{3/2}}{m_\rho^2} . \qquad (31)$$

TABLE II: Two pion energies in then A_2^- sector.

η	1.0	1.25	2.0
aE_0	0.516(10)	0.511(4)	0.442(4)
aE_1	0.660(6)	0.606(10)	0.549(12)
$\delta_1(E_0)$	1.71(11)	0.822(65)	0.242(31)
$\delta_1(E_1)$	2.99(10)	2.64(13)	2.04(18)
am_π	0.1925(7)	0.1944(6)	0.1946(8)

We find

$$g_{\rho\pi\pi} = 6.67(42) , \qquad m_\rho = 827(3)(5)\ \text{MeV} ,$$
$$\Gamma = 76.6(20)(5)\ \text{MeV} , \qquad \Gamma_{ph} = 184(23)\ \text{MeV} , \qquad (32)$$

where Γ_{ph} is computed using the computed value of $g_{\rho\pi\pi}$ and the physical values of m_ρ and m_π. The first quoted uncertainty indicates the statistical uncertainty, and the second indicates the uncertainty associated with the determination of the lattice spacing.

In Fig. 3 we show the scattering phase shifts and the fit curve we obtained using the effective range formula. With the exception of the left-most and right-most points, the data are not more than one standard deviation away from the curve. However, the confidence level of the fit is $Q \approx 8\%$, and it is not clear whether the effective range formula is reliable for $m_\pi = 304(2)$ MeV. Assuming the effective range formula is reliable, the value we computed for the coupling constant is in reasonably good agreement with the physical value quoted by the PDG $g_{\rho\pi\pi}^{phys} = 5.975(16)$ [15].

In Fig. 4 we compare our results to other recent lattice studies [9, 13, 21]. Our result for the coupling constant is in good agreement with other studies and was determined with similar precision. The value of m_ρ is also compatible with the value reported by the other studies, but our error bar is significantly smaller. We note that the results reported by Lang and collaborators [13] differ significantly from our results and the ones of other lattice studies. This is presumed to be due to the fact that the volume used in their study is too small.

The phase shifts and the values we obtained for m_ρ and $g_{\rho\pi\pi}$ are also in good agreement with one-loop unitarized chiral perturbation theory [14]. To show the agreement, in the left panel of Fig. 3 we plot the phase shift expected from unitarized χPT to $O(p^4)$ for $m_\pi = 304$ MeV. Note that this is not a fit to our data – the only input from our study to this expression is the pion mass. Another check
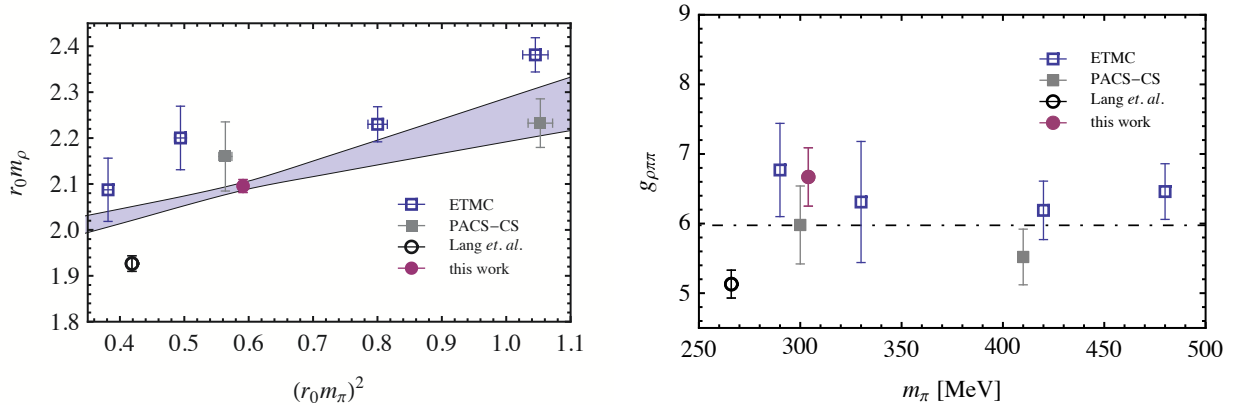
FIG. 4: Left panel: m_ρ versus m_π from recent lattice studies. We use lattice units to remove the uncertainty associated with setting the scale. The band represents the prediction from unitarized χPT [14] (note that this is not a fit to our data). Right panel: coupling as a function of m_π from recent lattice studies. The dot-dashed line is the PDG result [15].

is presented in the left panel of Fig. 4 where we plot the expectation for the mass of the ρ as a function of the pion mass. Our datapoint falls directly on top of the predicted band in the region where the unitarized χPT prediction has the smallest uncertainty. This is not a trivial agreement since this band has no input from our study.

IV. CONCLUSIONS

We presented the first study of the ρ meson decay using asymmetrical lattices. The calculation was carried out using nHYP-smeared clover fermions with two mass-degenerate quark flavors at a pion mass of $m_\pi = 304(2)$ MeV. We used three ensembles of 300 dynamical gauge configurations and computed the P-wave scattering phase shifts for the isospin $I = 1$ channel. Fitting the phase shifts using the effective range formula, we found a coupling constant $g_{\rho\pi\pi} = 6.67(42)$ and resonance mass $m_\rho = 827(3)(5)$ MeV. Using the computed value for the coupling constant and assuming that it does not change significantly as the quark mass is lowered towards the physical point, we estimate the physical decay width to be $\Gamma_{ph} = 184(23)$ MeV, which is compatible with the experimental value $\Gamma_{exp} = 149.1(8)$ MeV.

To compute the scattering phase shifts, we chose lattice volumes with one spatial direction elongated. By varying the elongation parameter, we were able to compute a set of scattering phase shifts evenly distributed throughout the spectral region where the ρ decays. While the moving frame formalism has been successfully used to study the ρ decay for as low as $m_\pi = 266$ MeV on cubic lattices, the finer momentum control offered by asymmetrical lattices will be needed to study narrower resonances.

We found that both the $\pi\pi(t)$ and $\rho(t)$ interpolators couple to the two-pion scattering states and can be used to extract the ground state. However, using the varia-

tional method allows both the ground and first excited state to be computed and gives a more precise determination of the ground state.

To compute the quark diagrams required for the two-pion operator, we had to employ stochastic methods. When employing spin-color dilution for the noise, we found that the gauge variance of the estimators is substantially larger than the noise variance. It is then sufficient to use only two independent noise vectors per configuration – additional vectors will add significantly to the analysis cost without reducing the final error bars.

To compute the resonances parameters, we used the effective range formula. While this formula described the overall phase shift profile well, the confidence level for our fit was only $Q \simeq 8\%$. We find that the effective range formula cannot reliably describe the phase shifts for the entire momentum range used in our study. However, the data points in the resonance region are well described by this formula.

Our results are compatible with most recent lattice studies and our error bars are comparable or better. Moreover, our results were in very good agreement with the predictions of unitarized chiral perturbation theory.

For future studies, we plan to increase the size of the variational basis as proposed by [10], include smeared quarks, and compute the resonance parameters at a pion mass $m_\pi \simeq 200$ MeV. The systematic effects due to lattice spacing, finite volume, and the inclusion of strange quark dynamics will be determined in further studies.

the unitarized χPT data. This work has been performed on the IAC cluster supported by the National Center for Supercomputing Applications, the HPCL clusters at The George Washington University, and the Keeneland Computing Facility at the Georgia Institute of Technology, which is supported by the National Science Foundation under Contract OCI-0910735. This work is supported in part by the U.S. Department of Energy grant DE-FG02-95ER-40907 and NSF CAREER grant PHY-1151648.

Appendix A: Numerical evaluation of $\mathcal{Z}_{lm}(s, q^2; \eta_2, \eta_3)$

In the following we describe the numerical evaluation of the generalized zeta functions defined by

$$\mathcal{Z}_{lm}(s, q^2; \eta_2, \eta_3) = \sum_{\mathbf{n} \in \mathbb{Z}^3} \frac{\mathcal{Y}_{lm}(\tilde{\mathbf{n}})}{(\tilde{\mathbf{n}}^2 - q^2)^s} \qquad (A1)$$

for

$$\mathrm{Re}\, 2s < l + 3 \,. \qquad (A2)$$

We use the same strategy originally proposed by Lüsher in [3]. Its extension to asymmetrical lattices is given in [7]. In the following, we give the relevant formulas, describe the numerical procedure used in this work, and give a list of values for comparison.

We begin by introducing the heat kernel

$$\mathcal{K}(t, \mathbf{x}) = \frac{1}{(2\pi)^3} \sum_{\mathbf{n} \in \mathbb{Z}^3} e^{i\tilde{\mathbf{n}} \cdot \mathbf{x} - t\tilde{\mathbf{n}}^2} \qquad (A3)$$

$$= \frac{\eta_2 \eta_3}{(4\pi t)^{3/2}} \sum_{\mathbf{n} \in \mathbb{Z}^3} e^{-\frac{1}{4t}(\mathbf{x} - 2\pi \hat{\mathbf{n}})^2} \qquad (A4)$$

where $\hat{\mathbf{n}} = (n_1, \eta_2 n_2, \eta_3 n_3)$ and $\tilde{\mathbf{n}} = (n_1, n_2/\eta_2, n_3/\eta_3)$. The first form is the definition of the heat kernel. Eq. (A4) follows from Eq. (A3) by applying the Poisson summation formula

$$\sum_{\mathbf{n} \in \mathbb{Z}^3} f(\mathbf{n}) = \sum_{\mathbf{k} \in \mathbb{Z}^3} \int_{-\infty}^{\infty} f(\mathbf{x}) e^{i2\pi \mathbf{k} \cdot \mathbf{x}} d^3x \qquad (A5)$$

and will be useful for small times t. The derivatives of the heat kernel are defined by

$$\mathcal{K}_{lm}(t, \mathbf{x}) = \mathcal{Y}_{lm}(-i\nabla_{\mathbf{x}}) \mathcal{K}(t, \mathbf{x}) \qquad (A6)$$

where the expression $\mathcal{Y}_{lm}(-i\nabla_{\mathbf{x}})$ is to be understood as the replacement of the homogeneous polynomial

$$\mathcal{Y}_{lm}(\mathbf{x}) = x^l Y_{lm}(\Omega_{\mathbf{x}}) \,, \qquad (A7)$$

using the rule $x_i \to \frac{\partial}{\partial x_i}$. Lastly, we define the truncated heat kernel and its derivatives as

$$\mathcal{K}^{\Lambda}(t, \mathbf{x}) = \mathcal{K}(t, \mathbf{x}) - \frac{1}{(2\pi)^3} \sum_{|\tilde{\mathbf{n}}| \leq \Lambda} e^{i\tilde{\mathbf{n}} \cdot \mathbf{x} - t\tilde{\mathbf{n}}^2} \,, \qquad (A8)$$

and

$$\mathcal{K}^{\Lambda}_{lm}(t, \mathbf{x}) = \mathcal{Y}_{lm}(-i\nabla_{\mathbf{x}}) \mathcal{K}^{\Lambda}(t, \mathbf{x}) \,. \qquad (A9)$$

A valid representation of the generalized zeta function, analytically continued to the half plane $\mathrm{Re}\, 2s > 1/2$, can be written in terms of the truncated heat kernel as

$$\begin{aligned}
&\mathcal{Z}_{lm}(s, q^2; \eta_2, \eta_3) \\
&= \sum_{|\tilde{\mathbf{n}}| \leq \Lambda} \frac{\mathcal{Y}_{lm}(\tilde{\mathbf{n}})}{(\tilde{\mathbf{n}}^2 - q^2)^s} + \frac{(2\pi)^3}{\Gamma(s)} \left\{ \frac{\delta_{l0}\delta_{m0}\eta_2\eta_3}{(4\pi)^2(s - 3/2)} \right. \\
&+ \int_0^1 dt\, t^{s-1} \left[e^{tq^2} \mathcal{K}^{\Lambda}_{lm}(t, \mathbf{0}) - \frac{\delta_{l0}\delta_{m0}\eta_2\eta_3}{(4\pi)^2 t^{3/2}} \right] \\
&\left. + \int_1^{\infty} dt\, t^{s-1} e^{tq^2} \mathcal{K}^{\Lambda}_{lm}(t, \mathbf{0}) \right\} \qquad (A10)
\end{aligned}$$

where the cutoff Λ is chosen such that $\Lambda^2 > \mathrm{Re}\, q^2$. In order to compute the scattering phase shifts, we need to evaluate $\mathcal{Z}_{lm}(1, q^2; \eta_2, \eta_3)$ numerically. In the following we describe the procedure used in this work.

For the case of interest, $s = 1$, we have

$$\begin{aligned}
&\mathcal{Z}_{lm}(1, q^2; \eta_2, \eta_3) \\
&= \sum_{|\tilde{\mathbf{n}}| \leq \Lambda} \frac{\mathcal{Y}_{lm}(\tilde{\mathbf{n}})}{(\tilde{\mathbf{n}}^2 - q^2)} + (2\pi)^3 \left\{ -\frac{\delta_{l0}\delta_{m0}\eta_2\eta_3}{8\pi^2} \right. \\
&+ \int_0^1 dt \left[e^{tq^2} \mathcal{K}^{\Lambda}_{lm}(t, \mathbf{0}) - \frac{\delta_{l0}\delta_{m0}\eta_2\eta_3}{(4\pi)^2 t^{3/2}} \right] \\
&\left. + \int_1^{\infty} dt\, e^{tq^2} \mathcal{K}^{\Lambda}_{lm}(t, \mathbf{0}) \right\} \,. \qquad (A11)
\end{aligned}$$

In order to evaluate $\mathcal{Z}_{lm}(1, q^2; \eta_2, \eta_3)$, the infinite sums appearing in $\mathcal{K}^{\Lambda}_{lm}(t, \mathbf{0})$ must be truncated. In the integration region $[1, \infty]$, we use Eq. (A3) to define $\mathcal{K}_{lm}(t, \mathbf{0})$. In this case subsequent terms in the sum are suppressed by $\mathrm{Re}\, e^{-t(\tilde{\mathbf{n}}^2 - q^2)}$, and the sum converges the slowest for $t = 1$. In the integration region $[0, 1]$, we use the alternative definition of the heat kernel to define $\mathcal{K}^{\Lambda}_{lm}(t, \mathbf{0})$. In this case one has to approximate $e^{tq^2} \mathcal{K}_{lm}(t, \mathbf{0})$. Again, the sum converges the slowest at $t = 1$ with successive terms being suppressed by $\mathrm{Re}\, e^{-\frac{(\pi\hat{\mathbf{n}})^2}{t} + tq^2}$. The cutoff is then chosen such that the integrands are approximated to a desired precisions for $t = 1$. In Table III we list some values for comparison, and in Figure 5 we plot $\mathcal{Z}_{00}(1, q^2; 1, 2)$ and $\mathcal{Z}_{20}(1, q^2; 1, 2)$ in the range $0 < q^2 < 4$.

q^2	$\mathcal{Z}_{00}(1, q^2, 1, 2)$	$\mathcal{Z}_{20}(1, q^2, 1, 2)$
0.2	6.35553	5.62348
0.41	-5.08222	-2.90547
0.62	1.16621	-2.22911
0.83	10.9025	-2.85516
1.04	-33.5287	-5.64013

TABLE III: A few values for $\mathcal{Z}_{00}(1, q^2, 1, 2)$ and $\mathcal{Z}_{20}(1, q^2, 1, 2)$.
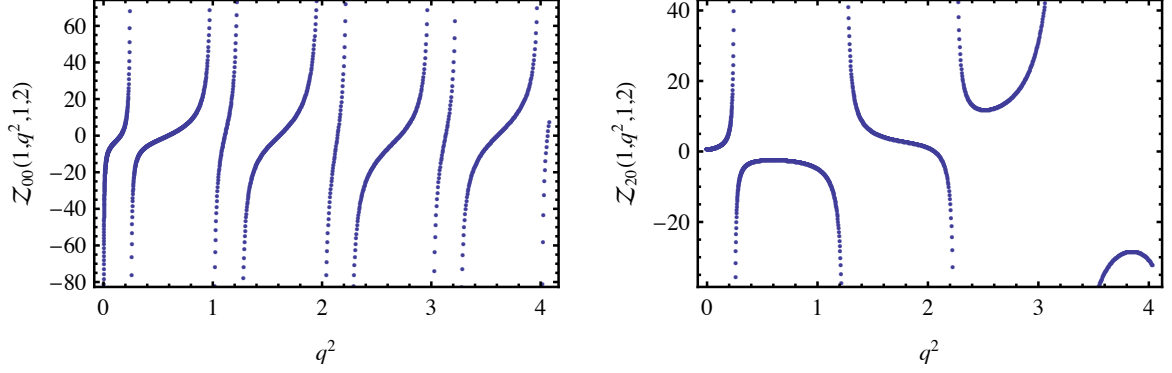
FIG. 5: $\mathcal{Z}_{00}(1, q^2, 1, 2)$ and $\mathcal{Z}_{20}(1, q^2, 1, 2)$.

Appendix B: Determination of the lattice spacing

To determine the lattice spacing, we use the Sommer scale [22]. We work in the Coulomb gauge and extract the heavy quark potential from the relation

$$\left\langle W_T^\dagger(\mathbf{x}, t) W_T(\mathbf{x} + \mathbf{r}, t) \right\rangle_U \approx c e^{-V(\mathbf{r})T} , \qquad \text{(B1)}$$

which is valid for large T with Wilson line W_T defined by

$$W_T(\mathbf{x}, t) = \prod_{i=0}^{T-1} U_4(\mathbf{x}, t + i) . \qquad \text{(B2)}$$

To fit the data, we use the functional form

$$V(r) = C + \frac{B}{r} + \sigma r + \lambda \left(\left. \frac{1}{r} \right|_{latt} - \frac{1}{r} \right) \qquad \text{(B3)}$$

where C is part of the quarks' self-energy, σ is the string tension, $B = -\frac{3}{4}\alpha_s$, and the last term is the difference between the lattice and continuum potentials. The Sommer parameter is then determined through

$$r_0/a = \sqrt{\frac{1.65 + B}{\sigma}} . \qquad \text{(B4)}$$

Using a combined fit to all three ensembles and averaging over all space-time points, we find

$$C = 0.919(4) , \quad B = -0.430(5) , \quad \sigma = 0.077(1), \qquad \text{(B5)}$$

and

$$r_0/a = 3.984(21) . \qquad \text{(B6)}$$

To fix the lattice spacing, we take $r_0 = 0.5$ fm and obtain $a = 0.1255(7)$ fm.

[1] M. Lüscher, *Commun. Math. Phys.* **104** (1986) 177.
[2] M. Lüscher, *Commun.Math.Phys.* **105** (1986) 153–188.
[3] M. Lüscher, *Nucl. Phys.* **B354** (1991) 531–578.
[4] M. Lüscher, *Nucl.Phys.* **B364** (1991) 237–254.
[5] L. Maiani and M. Testa, *Phys.Lett.* **B245** (1990) 585–590.
[6] K. Rummukainen and S. A. Gottlieb, *Nucl.Phys.* **B450** (1995) 397–436, [{\tthep-lat/9503028}].
[7] X. Li and C. Liu, *Phys.Lett.* **B587** (2004) 100–104, [{\tthep-lat/0311035}].
[8] X. Feng, X. Li, and C. Liu, *Phys.Rev.* **D70** (2004) 014505, [{\tthep-lat/0404001}].
[9] X. Feng, K. Jansen, and D. B. Renner, *Phys.Rev.* **D83** (2011) 094505, [{\ttarXiv:1011.5288}].
[10] S. Prelovsek, C. Lang, D. Mohler, and M. Vidmar, *PoS* **LATTICE2011** (2011) 137, [{\ttarXiv:1111.0409}].
[11] S. Aoki *et. al.* (**CP-PACS** Collaboration), [{\ttarXiv:1106.5365}].
[12] C. Pelissier, A. Alexandru, and F. X. Lee, *PoS* **LATTICE2011** (2011) 134, [{\ttarXiv:1111.2314}].
[13] C. B. Lang, D. Mohler, S. Prelovsek, and M. Vidmar,

[{\ttarXiv:1105.5636}].
[14] J. Pelaez and G. Rios, *Phys.Rev.* **D82** (2010) 114002, [{\ttarXiv:1010.6008}].
[15] K. Nakamura *et. al.* (**Particle Data Group** Collaboration), *J.Phys.* **G37** (2010) 075021.
[16] A. Ukawa (**CP-PACS and JLQCD** Collaboration), *Nucl.Phys.Proc.Suppl.* **106** (2002) 195–196.
[17] M. Lüscher and U. Wolff, *Nucl. Phys.* **B339** (1990) 222–252.
[18] B. Blossier, M. Della Morte, G. von Hippel, T. Mendes, and R. Sommer, *JHEP* **0904** (2009) 094, [{\ttarXiv:0902.1265}].
[19] A. Alexandru, C. Pelissier, B. Gamari, and F. Lee, *J. Comput. Phys.* **231** (2012) 1866–1878, [{\ttarXiv:1103.5103}].
[20] A. Hasenfratz, R. Hoffmann, and S. Schaefer, *JHEP* **05** (2007) 029, [{\tthep-lat/0702028}].
[21] S. Aoki *et. al.* (**CP-PACS** Collaboration), *PoS* **LAT2006** (2006) 110, [{\tthep-lat/0610020}].
[22] R. Sommer, *Nucl.Phys.* **B411** (1994) 839–854, [{\tthep-lat/9310022}].